Design of Cold-Formed Steel Built-Up I Section Columns subjected to Interactive Buckling

Sivaganesh Selvaraj[1], Mahendrakumar Madhavan[2]

Abstract

An experimental investigation into the behaviour of cold-formed steel (CFS) built-up I column assembly compressed between fixed ends is presented. To study the interactive buckling mode of failures, the built-up column assembly is designed to be doubly symmetric and locally slender. A total of forty-one columns were tested including different cross-section dimensions, lengths, intermediate connection spacing, and slendernesses. It is experimentally shown that the local buckling deformations caused the built-up cross-section assembly columns to fail predominantly in interactive local and flexural-torsional buckling. The influence of intermediate fastener spacing was also prevalent in the failure modes. The appropriateness of the AISI's maximum intermediate connection spacing limitation is verified to prevent global instability failures. The test and design results comparison indicated that the current AISI's DSM design curve for interactive buckling is unconservative for the CFS built-up columns with predominant interactive local-global failure mode vulnerability. Therefore, a modified design curve for interactive local-global buckling is proposed.

1 General

The CFS structures are becoming a common choice for construction due to their several advantages, but primarily due to is simple erection methods. The CFS structures are simple in geometry but complex in structural behaviour, the common failure modes are local ($f_{crl} < f_{crd}$, f_{cre} and f_y), distortional ($f_{crd} < f_{crl}$, f_{cre} and f_y), and global ($f_{cre} < f_{crl}$, f_{crd} and f_y), and either two of these failure modes or all of them can occur simultaneously ($f_y >> f_{crl} = f_{crd} = f_{cre}$). This complex structural behavioral feature led to overly safe design strength predictions by AISI [1]. The major complex failure modes in CFS structures are the buckling interactions [local-global (L-G), local-distortional (L-D), local-distortional-global (L-D-G), distortional-global (D-G) and global-global (flexural-torsional/flexural-FT-F)] due to higher slenderness or very similar slenderness in all three individual categories. This interactive buckling feature is closely related to the combination of its cross-section geometry (shape and dimensions), length, and support/bracing conditions. In the structural mechanical definition, when the post-buckling behaviour of a structural system involved deformations from more than one individual buckling (local, distortional or global) mode, it is called interaction buckling mode. The interaction buckling causes strength reduction in a structural system, neglecting this interaction effect will lead to unsafe design predictions. Thus, this complex structural behaviour is responsible for the fact that the recent North American

Design Specification for the Cold-Formed Steel Structural Members [2] does not adequately cover the various interactive buckling modes of built-up columns that fail in flexural-torsional modes combined with local buckling or global interactive flexural-torsional/flexural buckling due to intermediate connection spacing by means of the direct strength method (DSM) [3].

Over the past few decades, various researchers discovered the interactive buckling modes in CFS structural members and proposed a new design method. The local-distortional interaction buckling mode is notably one of the most thoroughly studied phenomena, through experimental, numerical, and design proposals [4-12]. The local-global interaction was well formulated for design by various researchers over several decades [8, 13]. A detailed discussion about the CFS cross-sections and their possible interactive failure modes and the reason for interaction is summarized in the latest state-of-the-art paper by Camotim et al. [14-15]. More recently, DSM based new design curves were developed to estimate the ultimate strength of (i) uniformly bent simply supported beams failing in distortional buckling and (ii) fixed ended columns failing in flexural torsional buckling modes by - more details about the research behind those proposals can be found in [16-19].

This paper investigates the interactive buckling failure modes of CFS back-to-back connected built-up assembly

---

[1] Postdoctoral fellow, Department of Civil and Environmental Engineering, The Hong Kong Polytechnic University, Hong Kong. sivaganesh.selvaraj@polyu.edu.hk
[2] Professor, Department of Civil Engineering, Indian Institute of Technology Hyderabad, Telangana, India. mkm@ce.iith.ac.in

using plain channels (U shape) subjected to axial compression (Fig. 1). The various failure modes of the built-up columns with corresponding ultimate axial strength are reported. The reason for interactive failure modes and their influence on the ultimate strength is summarized in detail. The failure mode behavior, the ultimate axial compression strengths of the built-up columns are compared with the AISI's DSM design predictions. Finally, the appropriateness of the current DSM equations for the local-global equation is verified. The experimental test-setup, material properties, geometric imperfection data and detailed failure mode investigations are presented in Selvaraj and Madhavan [16-17 and 20].
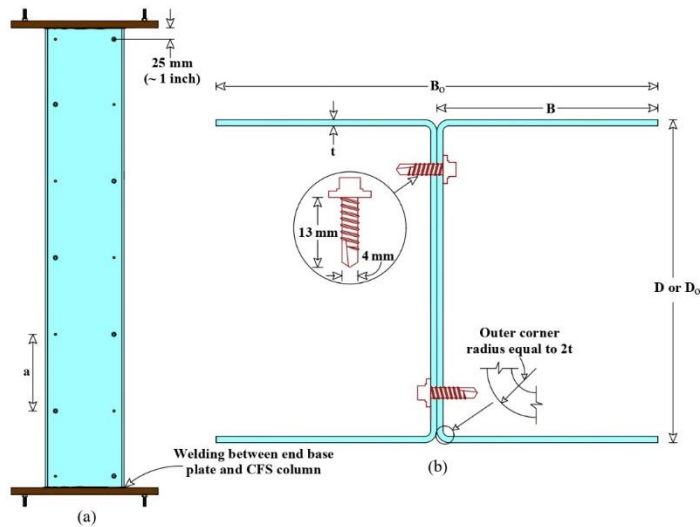

Fig. 1. Built-up cross-section assembly: (a) View of test specimen; (b) Cross-sectional view of back-to-back connected cross-section

2 Structural Behaviour of Built-up Column Assemblies and Discussions

The test results of the built-up column assemblies including failure modes and ultimate axial load (P_T) are summarized against the corresponding geometric properties such as [$(a/r_i)/(KL/r)_o$], $L/(B_b/2)$ and slendernesses (λ_l, λ_{l-e}, and λ_e) in Tables 1-2. The observed failure mode photographs and axial load versus axial deformation curves for all the tested built-up column assemblies are shown in Figs. 2. A more detailed discussion about the structural behaviour and failure modes including Integrity of the built-up columns is described in [16]. In general, the test results indicate that the failure modes are significantly influenced by the built-up column assembly geometry resulting in an interactive buckling feature. Further, it was also observed that the increase in intermediate connection fastener spacing (a) in the built-up cross-section assembly with high local slenderness (λ_l) increases the possibility of local-global interactive buckling. Except for one specimen, all other built-up column assemblies failed in interactive local-global buckling. Some specimens with intermediate connection

fastener spacing higher than the AISI limit [$(a/r_i)/(KL/r)_o > 0.5$] did not fail in individual flexural buckling (IFB).

Overall, the following failure modes were observed in the tests (i) interactive local and flexural torsional buckling of the overall built-up cross-section assembly (LB+FTB); (ii) interactive local and flexural buckling of the overall built-up cross-section assembly (LB+OFB); (iii) flexural buckling of the individual cross-section (IFB); and (iv) interactive local and flexural buckling of the individual cross-section (LB+IFB). In addition, susceptibly a new interactive buckling feature which is an interaction between local and flexural torsional buckling of the individual section (LB+IFTB) was also observed in a few specimens. The failure modes of the built-up column assemblies were observed throughout the loading until failure. The failure mode which occurred at the ultimate load was considered as the governing buckling of the built-up column assembly.

(a)   (b)   (c)   (d)

Fig. 2. Failure modes of 50/100-1800 set specimens: (a) 50/100-1800-L/10 specimen; (b) 50/100-1800-L/6 specimen; (c) 50/100-1800-L/2 specimen; (d) 50/100-1800-L/2 specimen-separation failure;

Though all the forty-one CFS built-up cross-section column assemblies are doubly symmetric and vulnerable to fail in local buckling ($\lambda_l > 1.5$) (Table 1), it is worth noting that forty among those failed in interactive local-flexural buckling (OFB or FTB or IFB or IFTB) as observed during the test (Fig 2 – read [16] for details). As expected, local buckling on the unstiffened flanges of the built-up column assembly was observed in the elastic loading stage in all the specimens except in specimen 120/70-1500-L/2. This may be

attributed to the fact that the specimen 120/70-1500-L/2 has the highest global slenderness with larger interconnection spacing (L/2). Further, the local buckling wave magnitudes increased gradually as the load reached the ultimate and post-peak zone. In the case of interaction between local buckling and overall flexural buckling (OFB), the local buckling shape became localized near the mid-length on the compressed side.

Table 1. Geometric properties and Experimental results of Cold-formed steel built-up column assemblies

Specimen	(a/r_i) / $(KL/r)_o$	Slenderness			Experimental results		P_{nl} (kN) (Eq. 1)	P_T / P_{nl}
		λ_l	$\lambda_{l\text{-}e}$	λ_e	P_T (kN)	Failure mode		
70/110-1800-L/10	0.28	1.73	1.64	0.53	106.00	LB+OFB	114.35	0.93
70/110-1800-L/8	0.35		1.64	0.53	93.82	LB+OFB		0.82
70/110-1800-L/6	0.47		1.64	0.53	92.06	LB+OFB		0.81
70/110-1800-L/4	0.70		1.62	0.58	89.62	LB+OFB		0.78
70/110-1800-L/2	1.40		1.51	0.82	84.45	LB+IFTB		0.74
70/110-1400-L/10	0.28		1.67	0.42	109.73	LB+FTB		0.96
70/110-1400-L/8	0.35		1.67	0.42	107.13	LB+FTB		0.94
70/110-1400-L/6	0.47		1.67	0.42	99.97	LB+FTB		0.87
70/110-1400-L/4	0.70		1.66	0.45	95.67	LB+FTB		0.84
70/110-1400-L/2	1.40		1.59	0.64	90.20	LB+IFTB		0.79
70/110-1000-L/10	0.28		1.70	0.30	112.64	LB+OFB		0.99
70/110-1000-L/8	0.35		1.70	0.30	110.44	LB+OFB		0.97
70/110-1000-L/6	0.47		1.70	0.30	101.56	LB+OFB		0.89
70/110-1000-L/4	0.70		1.70	0.32	98.51	LB+OFB		0.86
70/110-1000-L/2	1.40		1.66	0.46	90.69	LB+IFTB		0.79
100/80-1400-L/10	0.25	1.52	1.40	0.62	94.64	LB+OFB	125.85	0.75
100/80-1400-L/6	0.42		1.39	0.65	93.58	LB+OFB		0.74
100/80-1400-L/2	1.27		1.25	0.97	82.36	LB+IFB		0.65
100/80-1000-L/10	0.25		1.45	0.44	102.64	LB+OFB		0.82
100/80-1000-L/6	0.42		1.45	0.46	93.26	LB+OFB		0.74
100/80-1000-L/2	1.27		1.37	0.69	87.22	LB+IFB		0.69
50/100-1800-L/10	0.26	1.54	1.47	0.64	79.29	LB+FTB	102.87	0.88
50/100-1800-L/6	0.44		1.47	0.64	69.27	LB+FTB		0.77
50/100-1800-L/2	1.32		1.33	0.94	68.65	LB+IFTB		0.87
50/100-1000-L/10	0.26		1.50	0.37	96.17	LB+OFB		0.93
50/100-1000-L/6	0.43		1.50	0.37	92.95	LB+OFB		0.90
50/100-1000-L/2	1.30		1.46	0.52	89.22	LB+IFTB		0.87
50/130-1800-L/10	0.21	1.97	1.84	0.59	95.82	LB+FTB	105.08	0.91
50/130-1800-L/8	0.26		1.84	0.59	90.37	LB+FTB		0.86
50/130-1800-L/6	0.34		1.84	0.59	89.15	LB+FTB		0.85
50/130-1800-L/4	0.51		1.82	0.62	87.46	LB+FTB		0.83
50/130-1800-L/2	1.03		1.73	0.79	87.32	LB+FTB		0.83
50/130-1200-L/8	0.26		1.91	0.40	97.63	LB+FTB		0.93
50/130-1200-L/6	0.34		1.91	0.40	95.54	LB+FTB		0.91
50/130-1200-L/4	0.51		1.90	0.41	88.46	LB+FTB		0.84
50/116-1200-L/10	0.28	1.56	1.51	0.41	91.29	LB+OFB	108.74	0.84
50/116-1200-L/2	1.42		1.45	0.60	84.6	LB+IFTB		0.78
120/70-1500-L/10	0.24	1.67	1.40	0.92	78.83	LB+OFB	121.95	0.65
120/70-1500-L/8	0.30		1.39	0.93	77.53	LB+OFB		0.64
120/70-1500-L/4	0.60		1.33	1.04	74	LB+OFB		0.61
120/70-1500-L/2	1.21		1.11	1.40	74.01	IFB		0.61

Note: Actual dimensions of the columns can be obtained from the original paper [16]. $\lambda_{l\text{-}e} = (\sigma_{cre}/\sigma_{crl})^{0.5}$ [modified version is given in Eq. (3) and Eq. (7)]; LB - Local buckling; OFB - Flexural buckling of the built-up section as a whole; FTB - Flexural torsional buckling of the built-up section as a whole; IFB – Flexural buckling of the individual section; IFTB - Flexural torsional buckling of the individual section; P_T - Ultimate axial strength of the built-up CFS column; P_{nl} - Axial strength for local buckling

Although the experimental failure modes show a clear indication of interaction buckling (local + global mode), it is necessary to confirm the same through design methods before interpreting the possible reason for various interaction failure modes. The interaction of bucking modes can be endorsed if the ultimate axial compression strength of the column obtained from the tests is lesser than the individual buckling curve strength because the buckling interaction reduces the strength of the member. For the design purpose, the individual local buckling curve of AISI's DSM is used. The nominal axial strength of the CFS built-up column for individual local buckling can be determined using Eqs. (1).

$$P_{nl} = \begin{cases} P_y & \text{if } \lambda_l \leq 0.776 \\ P_y \left(\frac{P_{crl}}{P_y}\right)^{0.4} \left[1 - 0.15\left(\frac{P_{crl}}{P_y}\right)^{0.4}\right] & \text{if } \lambda_l > 0.776 \\ \lambda_l = \left(P_y/P_{crl}\right)^{0.5} \text{ [local buckling]} \end{cases} \quad (1)$$

Where P_{nl} is the nominal axial compression strength for local buckling, P_y is the axial compression strength for yield stress (cross-sectional area x yield stress), P_{crl} is the elastic critical buckling stress for local buckling that can be determined from THINWALL software already cited. It should be noted that the elastic critical local buckling stress (P_{crl}) should be obtained from the elastic buckling curve of individual cross-section as per the suggestions of Young and Chen [13] and Selvaraj and Madhavan [9-12].
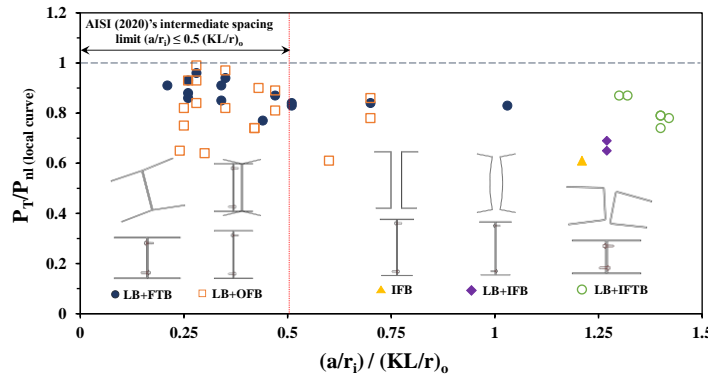

Fig. 3. Comparison of local buckling design strength and failure modes concerning the change in (a/r_i) / (KL/r)$_o$ ratio

The comparison between the individual local buckling strength (P_{nl}) and test results (P_T) indicates that all the predicted columns strength using Eq. (1) is higher than the test results as shown in Table 1 and Figure 3 (all P_T/P_{nl} ratios are less than unity). This indicates that the actual ultimate buckling strength of the locally slender ($\lambda_l > 1.5$) built-up column assemblies is reduced possibly because of interaction from other buckling modes. More detailed investigations about the failure modes of built-up column assemblies and interpretation of the AISI design methods are discussed in the following sections.

3 Local buckling induced Flexural Buckling modes on fixed end doubly symmetric columns

The geometric configurations of the built-up column assemblies investigated in the present study are almost the same (all are back-to-back connected at the webs forming doubly symmetric cross-sections), however, the aspect ratio (overall depth (D_o) to breadth (B_o) ratio) varies thereby creating different possibilities for global buckling failure. This possibility of global buckling failure further increases with the influence of local buckling (λ_l) and intermediate connection spacing (a) in the doubly symmetric built-up cross-sections. It is also suspected that the local imperfections type (flare) may also induce higher magnitude local buckling leading to flexural torsional buckling. A detailed explanation about the reason for flexural torsional buckling in the double symmetric built-up column assemblies with fixed ends is explained as follows.

In fact, as per the research by Loughlan and Nabavian [21] and Mulligan and Pekoz [22], local buckling in doubly symmetric CFS cross-section will not influence global failure as the redistribution of local buckling stresses are symmetric about the overall centroid of the cross-section so the line of action of internal forces remains unchanged. Further, the research by Young and Rasmussen [23 and 24], Rasmussen and Hancock [25] concluded that the local buckling failure in fixed-end columns will not induce global failures. This was discovered in Young and Rasmussen [23-24] and Rasmussen and Hancock [25] by observing the load-displacement plots of fixed end columns and pinned end columns. However, the research from the present study indicates that the local buckling in fixed end columns also influences the global instability failures.

In a first, the built-up cross-section assembly with the lowest D_o/B_o ratio of 0.38 (50/130 set specimens) fails due to a combination of local buckling and flexural torsional buckling (LB+FTB), irrespective of the length Table 1. This is caused by the highest local slenderness ($\lambda_l = 1.97$) inducing local buckling. Due to the nature of the highly slender unstiffened flanges along the entire length of the column with vulnerability to local flare imperfection, the local buckling mode could be unsymmetric in the doubly symmetric built-up assembly cross-section. This unsymmetric local buckling led to the unsymmetric redistribution of longitudinal stress resulting in a shift in the line of action of the internal force (center of gravity). This shift in the center of gravity creates overall eccentricity in the column member and induces flexural torsional buckling even in the doubly symmetric cross-section assemblies. The influence of local buckling can be further observed from the load versus deformation plot of 50/130 set specimens, where the load versus deformation curves are losing stiffnesses at 70-80% of the ultimate load of the corresponding columns [read 16]. Though, these built-up cross-sections are designed to fail in

local buckling, the combined effect of low D_o/B_o ratio (0.38) and high local slenderness ($\lambda_l > 1.5$) resulted in interactive LB+FTB failure mode. This interaction also reduced the strength of the column (P_T) compared to the local buckling design strength (P_{nl}) by 7-17% as shown in Table 1 (see the ratio of P_T/P_{nl} in 50/130 set specimens).

Next, the built-up cross-section assemblies with higher D_o/B_o ratios of 1.25 and 1.71 (80/100 set and 120/70 set specimens, respectively) failed due to a combination of local buckling and overall flexural buckling (LB+OFB), as shown in Table 1. While, in the same set of specimens, the high global slenderness and larger interconnection spacing (L/2) influenced the columns to fail in LB+IFB and IFB in 100/80 set and 120/70 set, respectively (Table 1). These 100/80 and 120/70 set specimens are also vulnerable to failure in individual flexural buckling due to the very high depth to breadth ratio (D/B) of individual cross-sections. Therefore, these columns fail due to the separation of two individual sections with large lateral displacements. The combined effect of individual flexural buckling and local buckling ($\lambda_l =$ 1.52 and 1.67) reduced the strength of the built-up column (P_T) significantly by 18-39% compared to the local buckling strength (P_{nl}) as shown in Table 1 (see the ratio of P_T/P_{nl} for 100/80 set and 120/70 set specimens).

The specimens with intermediate-range of D_o/B_o ratios (0.43, 0.50, and 0.64) failed concerning their local slenderness and $(a/r_i)/(KL/r)_o$ ratios, the failure modes are LB+OFB, LB+FTB, and LB+IFTB. This intermediate column behaviour is complicated as the $(a/r_i)/(KL/r)_o$ increases beyond 0.5. When the $(a/r_i)/(KL/r)_o$ ratio is high (1.3 to 1.42 in the tested samples) in the intermediate range of D_o/B_o ratios (0.43, 0.50, and 0.64), all the specimens failed in flexural torsional buckling of individual sections. This failure mode can be further explained that the individual cross-section in the built-up assembly failed in flexural torsional buckling within the intermediate fastener connection spacing. The occurrence of this failure IFTB mode is a gradual process, (i) first due to the higher local slenderness, the local buckling occurs in the initial loading stage at the unstiffened flanges (Fig. 4b), (ii) then shift in the line of action of the internal force (change in center of gravity leading to load eccentricity) occurs which is caused simultaneously by unsymmetric redistribution of longitudinal stress, separation of individual cross-sections due to higher $(a/r_i)/(KL/r)_o$ ratio, and magnitude of local imperfection (flare) (Fig. 4c) (iii) finally the individual cross-section buckles in flexural torsional buckling due to the large slenderness and loading eccentricity (Fig. 4d). The separation of the individual cross-section could also happen in opposite directions (movement and twist in opposite directions) and so it might look like an overall flexural torsional buckling as well (two possible modes are shown in Fig. 4d). This complex interaction

behavior can also be observed in the form of stiffness drop in load versus deformation plots. These interactive failures reduced the actual strength of the column by a maximum of 26% compared to the local buckling strength as shown in Table 1 (see the ratio of P_T/P_{nl} for 70/110, 50/100, and 50/116 set specimens).

As the influence of various global instability failures (FTB, OFB, IFB, IFTB) are evident and predominant in the locally slender doubly symmetric built-up assemblies, the strength reduction must be incorporated in the AISI design specifications. Therefore, in the present investigation, the appropriateness of the current AISI design provisions is verified against the test results, and necessary modifications are made for effective and safe design strength predictions.

4 Effect of higher local slenderness on AISI's intermediate connection spacing limitations

The current AISI's limitations for intermediate fastener connection spacing for built-up column assembly $[(a/r_i) \leq 0.5 (KL/r)_o]$ is based on the hot-rolled steel column research primarily to prevent individual global buckling. Among the 41 tested columns, only 25 are complying with the AISI's spacing limit, while the 16 columns are designed purposefully to investigate the failure modes. In all the CFS built-up assemblies, the occurrence of interactive buckling is predominant and reduces the strength of the individual buckling mode. Hence, the question arises whether the spacing limitations of AISI $[(a/r_i) \leq 0.5 (KL/r)_o]$ are appropriate for the column buckling in interaction buckling modes. The following section interprets the effect of higher local slenderness on AISI's intermediate connection spacing limitations.

The variation in global failure modes concerning the $(a/r_i)/(KL/r)_o$ ratios is illustrated in Figure 3. It clearly indicates that the AISI's maximum intermediate connection spacing limitation $[(a/r_i) \leq 0.5 (KL/r)_o]$ is appropriate (overly safe) to prevent global instability failures (individual section buckling) in the built-up assemblies with predominant interactive failure mode vulnerability. The individual flexural buckling (IFB) occurred only on the specimens with $(a/r_i)/(KL/r)_o$ ratio higher than 1.03, which is two times higher than the maximum limit suggested AISI S100 (2020). Though this result is overly safe, this should be attributed to the influence of higher local buckling slenderness whose strength could be less than the global buckling strength for individual buckling. Therefore, it can be concluded that the AISI's maximum spacing limitation $[(a/r_i) \leq 0.5 (KL/r)_o]$ is appropriate for CFS built-up assembly vulnerable to interactive local-global failures.

Table 2. Comparison between Test results and DSM strength predictions

Specimen	P_T (kN)	Failure mode	P_{DSM} (kN) (Eq. 3)	P_{DSM}^M (kN) (Eq. 7)	P_T / P_{DSM}	P_T / P_{DSM}^M
70/110-1800-L/10	106.00	LB+OFB	106.02	86.14	1.00	1.23
70/110-1800-L/8	93.82	LB+OFB	106.02	86.14	0.88	1.09
70/110-1800-L/6	92.06	LB+OFB	106.02	86.14	0.87	1.07
70/110-1800-L/4	89.62	LB+OFB	104.31	85.12	0.86	1.05
70/110-1800-L/2	84.45	LB+IFTB	95.22	79.55	0.89	1.06
70/110-1400-L/10	109.73	LB+FTB	109.11	87.98	1.01	1.25
70/110-1400-L/8	107.13	LB+FTB	109.11	87.98	0.98	1.22
70/110-1400-L/6	99.97	LB+FTB	109.11	87.98	0.92	1.14
70/110-1400-L/4	95.67	LB+FTB	108.17	87.42	0.88	1.09
70/110-1400-L/2	90.20	LB+IFTB	102.38	83.95	0.88	1.07
70/110-1000-L/10	112.64	LB+OFB	111.60	89.45	1.01	1.26
70/110-1000-L/8	110.44	LB+OFB	111.60	89.45	0.99	1.23
70/110-1000-L/6	101.56	LB+OFB	111.60	89.45	0.91	1.14
70/110-1000-L/4	98.51	LB+OFB	111.16	89.19	0.89	1.10
70/110-1000-L/2	90.69	LB+IFTB	108.08	87.37	0.84	1.04
100/80-1400-L/10	94.64	LB+OFB	113.42	97.03	0.83	0.98
100/80-1400-L/6	93.58	LB+OFB	112.16	96.22	0.83	0.97
100/80-1400-L/2	82.36	LB+IFB	97.45	86.41	0.85	0.95
100/80-1000-L/10	102.64	LB+OFB	119.35	100.83	0.86	1.02
100/80-1000-L/6	93.26	LB+OFB	118.67	100.40	0.79	0.93
100/80-1000-L/2	87.22	LB+IFB	110.51	95.14	0.79	0.92
50/100-1800-L/10	79.29	LB+FTB	89.98	75.83	0.85	1.05
50/100-1800-L/6	69.27	LB+FTB	89.98	75.83	0.74	0.91
50/100-1800-L/2	68.65	LB+IFTB	79.04	68.76	0.82	1.00
50/100-1000-L/10	96.17	LB+OFB	99.15	82.96	0.97	1.16
50/100-1000-L/6	92.95	LB+OFB	99.15	82.96	0.94	1.12
50/100-1000-L/2	89.22	LB+IFTB	95.68	80.78	0.93	1.10
50/130-1800-L/10	95.82	LB+FTB	95.73	74.73	1.00	1.28
50/130-1800-L/8	90.37	LB+FTB	95.73	74.73	0.94	1.21
50/130-1800-L/6	89.15	LB+FTB	95.73	74.73	0.93	1.19
50/130-1800-L/4	87.46	LB+FTB	94.75	74.18	0.92	1.18
50/130-1800-L/2	87.32	LB+FTB	88.79	70.75	0.98	1.23
50/130-1200-L/8	97.63	LB+FTB	100.67	77.50	0.97	1.26
50/130-1200-L/6	95.54	LB+FTB	100.67	77.50	0.95	1.23
50/130-1200-L/4	88.46	LB+FTB	100.36	77.33	0.88	1.14
50/116-1200-L/10	91.29	LB+OFB	103.90	86.79	0.88	1.05
50/116-1200-L/2	84.6	LB+IFTB	98.59	83.44	0.86	1.01
120/70-1500-L/10	78.83	LB+OFB	97.06	83.03	0.81	0.95
120/70-1500-L/8	77.53	LB+OFB	96.37	82.59	0.80	0.94
120/70-1500-L/4	74	LB+OFB	90.81	78.94	0.81	0.94
120/70-1500-L/2	74.01	IFB	71.43	65.48	1.04	1.13
Mean (P_m)					0.90	1.10
Standard Deviation (s_t)					0.072	0.109
Coefficient of Variation (V_p)					0.080	0.099
Reliability Index (β_1) (according to ASCE 2010)[a] [26]					2.39	3.25
Reliability Index (β_2) (according to AS/NZS 2002)[a] [27]					2.43	3.30

Note: Actual dimensions of the columns can be obtained from the original paper [16]. The Reliability indices are calculated only for the specimens that comply with the AISI's maximum spacing limitation [$(a/r_i) \leq 0.5 \ (KL/r)_o$]; P_T - Ultimate axial strength of the built-up CFS column; P_{DSM} - Design strength of the column from Eq. (3); P_{DSM}^M - Design strength of the column from Eq. (7);

(a) Ideal column

(b) Buckling failure of a column when "a" is small (a = L$_{crl}$)

(b) Buckling failure of a column when "a" is large (a = L/2)

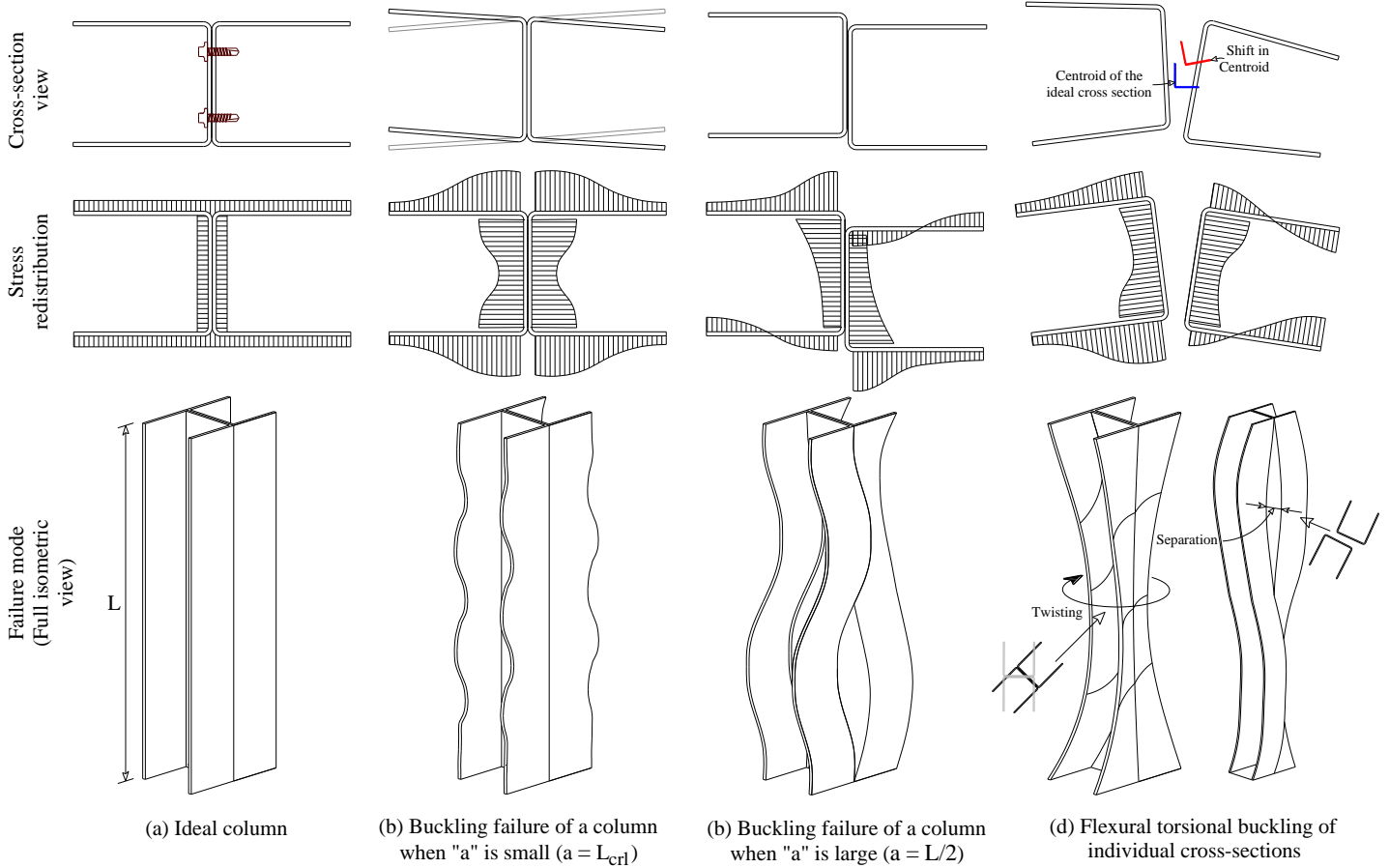(d) Flexural torsional buckling of individual cross-sections

Fig. 4. Step-by-step illustration of interactive local and flexural torsional buckling in individual cross-sections (LB+IFTB)

5 Direct Strength Method for Built-up Assembly Subjected to Axial Compression

Having confirmed the interactive local-global failure modes in built-up doubly symmetric column assemblies and the appropriateness of the AISI's spacing limitations, the next step is to verify the DSM interactive buckling expressions for accurate design strength predictions. The design expressions of the direct strength method (DSM) of AISI (2020) for CFS axial compression members are shown in Eqs (2-6). The appropriateness of these empirical expressions is verified against the test and numerical results by various researchers since discovered. The nominal axial compression strength of the CFS built-up column member (P_{DSM}) (Eq. 2) is the minimum of nominal strength for interactive local-global buckling (P_{nle}), and flexural/flexural-torsional buckling (P_{ne}). The distortional buckling is not considered as it was not observed in tests.

$$P_{DSM} = \min (P_{nle}, P_{ne}) \qquad (2)$$

The nominal axial strength of the CFS built-up column assembly for interactive local-global buckling ($\lambda_{l\text{-}e}$) can be determined using Eqs. (3).

$$P_{nle} = \begin{cases} P_{ne} & \text{if } \lambda_{l-e} \leq 0.776 \\ P_{ne} \left(\frac{P_{crl}}{P_{ne}}\right)^{0.4} \left[1 - 0.15 \left(\frac{P_{crl}}{P_{ne}}\right)^{0.4}\right] & \text{if } \lambda_{l-e} > 0.776 \quad (3) \\ \lambda_{l-e} = (P_{ne}/P_{crl})^{0.5} \text{ [local} - \text{global interactive bucking]} \end{cases}$$

Where P_{ne} and P_{nle} are the nominal axial strength for global buckling and local-global interactive buckling, P_{crl} is the elastic critical buckling stress for local buckling that can be determined from Thinwall software using individual cross-section section according to Young and Chen [13] and Selvaraj and Madhavan [9-12] and P_{ne} is from Eq. (4).

The nominal axial strength of the CFS built-up column assembly for flexural buckling/flexural torsional buckling (P_{ne}) can be determined in accordance with the Eq. (4)

$$P_{ne} = \begin{cases} P_y \left(0.658^{\lambda_e^2} \right) & \text{if } \lambda_e \leq 1.5 \\ P_y \left(\frac{0.877}{\lambda_e^2} \right) & \text{if } \lambda_e > 1.5 \\ \qquad \lambda_e = \left(P_y / P_{cre} \right)^{0.5} \end{cases} \qquad (4)$$

Where P_{cre} is the critical elastic global buckling load (F_{cre} multiplied by gross cross-sectional area), F_{cre} is the critical elastic global buckling stress (flexural or flexural torsional) and is taken as equal to the minimum of Eq. (5) and (6), the Eq. (5) encompasses with modified global slenderness to account for the effect of intermediate fastener spacing (a). The use of minimum F_{cre} value among Eq. (5) and (6) will lead to conservative design predictions as the tested samples are evidently failing in local buckling with global instability.

Elastic flexural buckling stress (E2.1 of AISI 2020)

$$F_{cre} = \frac{\pi^2 E}{(KL/r)^2} \qquad (5)$$

Elastic flexural torsional buckling stress (E2.2 of AISI 2020)

$$F_{cre} = \frac{1}{Ar_0^2} \left[GJ + \frac{\pi^2 E C_w}{(K_t L_t)^2} \right] \qquad (6)$$

Where E is the modulus of elasticity, K and K_t are the effective length factor for flexural buckling and twisting, respectively (chapter C of AISI 2020), L and L_t are the unbraced length of the member for flexural buckling and twisting, respectively, (KL/r) in the Eq. (5) shall be replaced by a term $(KL/r)_m$ to incorporate the effect of intermediate fastener spacing (a) in the critical elastic global buckling stress. A is the gross area of built-up assembly, r_0 radius of gyration (built-up), G is the shear modulus, J is the torsional constant (built-up) and C_w is the warping constant of the built-up cross-section.

The determined nominal axial compressive strengths [P_{DSM}] for all the tested columns are compared against the ultimate axial compression load obtained from the tests (P_T) as shown in Table 2. It is observed from the design calculation that the DSM method rightly predicted the failure mode as local-global interaction as P_{nle} (Eq. 3) is minimum for all the columns compared to the P_{ne} (Eq. 4), however the interactive local-global [Eqs. (3)] curve of AISI is unconservative by a maximum of 26% (P_T/P_{DSM}= 0.74). The mean value of the P_T/P_{DSM} ratio is 0.9 with a standard deviation (s_t) and coefficient of variation (V_p) values 0.072 and 0.080, respectively as can be observed from Table 2. The local buckling curve of the DSM is usually over-safe for highly slender sections (current λ_l is ranging from 1.52 to 1.97 and $\lambda_{l\text{-}e}$ is ranging from 1.11 to 1.91). However, the present investigation indicates that the global instability (flexural-torsional buckling) has reduced the ultimate

strength (P_T) of the tested columns leading to nonconservative design predictions ($P_T/P_{DSM} < 1$.

In the present investigation, the unconservative design prediction is present throughout the local slenderness range ($\lambda_{l\text{-}e}$ = 1.11 to 1.91) considered as shown in Fig. 5a. Therefore, to account for the interactive local-global behavioral feature of the built-up column, the current interactive design curve is modified. The modified design curve (P_{DSM}^M) for interactive [local-global (flexural)] buckling is shown below

$$P_{nle} = \begin{cases} P_{ne} & \text{if } \lambda_{l\text{-}e} \leq 0.776 \\ P_{ne} \left(\frac{P_{crl}}{P_{ne}} \right)^{0.6} \left[1 - 0.2 \left(\frac{P_{crl}}{P_{ne}} \right)^{0.6} \right] & \text{if } \lambda_{l\text{-}e} > 0.776 \\ \lambda_{l\text{-}e} = (P_{ne}/P_{crl})^{0.5} \text{ [local} - \text{global interactive bucking]} \end{cases} \qquad (7)$$

The current AISI curve Eq. (3) is modified only in the second part of the equation ($\lambda_{l\text{-}e} > 0.776$) with a new coefficient and exponent terms, the coefficient 0.15 is changed as 0.2 and the exponent term 0.4 is changed to 0.6. The slenderness limit of Eq. (3) remains the same in the modified interactive local buckling curve Eq. (7), as the current investigation is only beyond the slenderness range of 0.776.

The comparison between design prediction (P_{DSM}^M) as per the modified design curve (Eq. 7) and experimental test results are shown in Table 2 and Fig. 5b. It indicates that the design prediction is mostly safe and the maximum unconservativeness is only 9% (least P_T/P_{DSM}^M = 0.91 for 50/100-1800-L/6; mean P_T/P_{DSM}^M = 1.10) which is negligible and can be nullified when adopted with the resistance factor (ϕ = 0.85). Though the magnitude is negligible, the author's understanding is that the unconservativeness of the modified design curve (Eq. 7) is only in nine of the forty-one tested specimens and this can be nullified with the resistance factors are included for design strength predictions.

6   Reliability Analysis

Reliability analysis was carried out to assess the suitability of using the modified interactive design curve for the CFS doubly-symmetric cross-section built-up columns. The suitability of the design curves is assessed by a reliability index (β). It can be proved that the design curves are suitable for the use of design application when the calculated reliability index (β) is equal to or higher than the target reliability index (β_o = 2.5) value recommended in Section K2.1.1 (c) in AISI (2020) for structural members. The Reliability indices are calculated only for the specimens (only for 25 among the 41 specimens tested) that comply with the AISI's maximum spacing limitation [(a/ri) ≤ 0.5 $(KL/r)_o$] (Table 2). The required and appropriate statistical parameters for the reliability index calculation are obtained from Table K2.1.1-1 of AISI (2020).
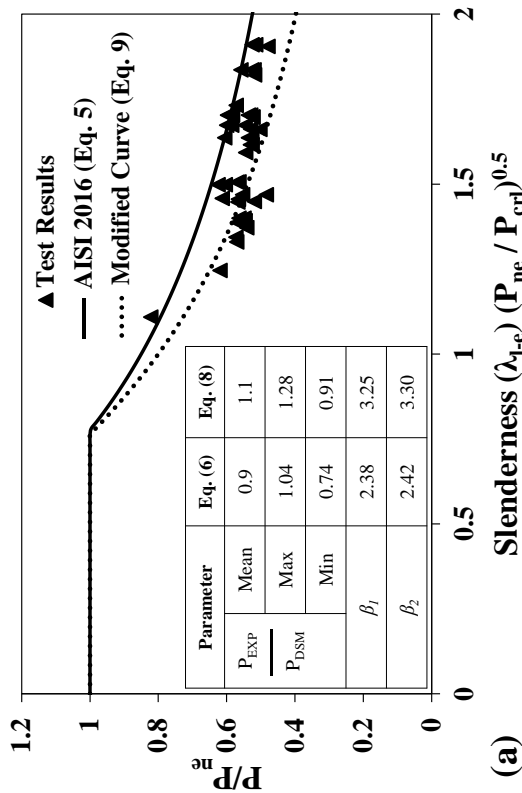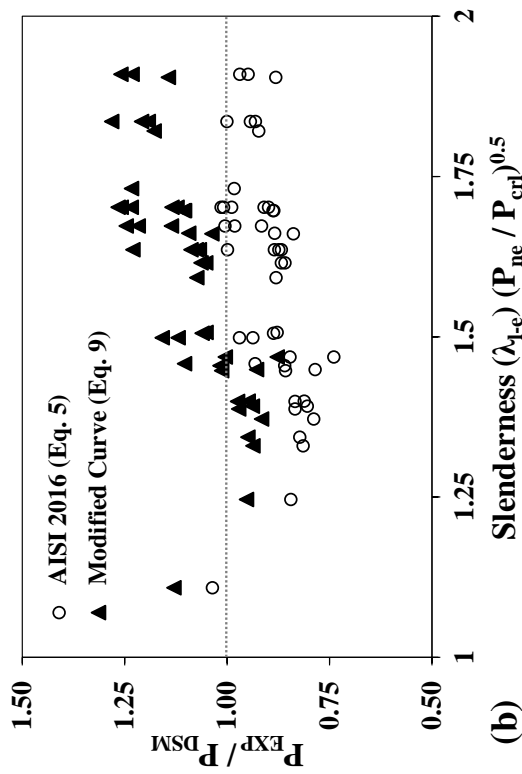
The statistical parameters are the mean (terms with subscript 'm') and coefficient of variation (V) for material and fabrication factor, they are $M_m=1.10$, $F_m=1.00$, $V_M=0.10$, and $V_F=0.05$. The ratios of P_T/P_{DSM} and P_T/P_{DSM}^M are used to calculate the statistical parameters to account for the experimental test results coefficient of variation (V_p) and mean value (P_m) as the coefficient of variation value is higher than 0.065 (AISI 2016). It should be noted that the resistance factor (ϕ) was not used in the reliability index calculation for conservativeness.

The reliability analysis indicates that the current AISI design curve [Eq. (3)] is unreliable for the design of CFS doubly symmetric built-up column with interactive buckling modes [β_1 and β_2 values of P_T/P_{DSM} is 2.39 and 2.43, respectively and less than the target reliability index (β_o)] (Table 2). Whereas the reliability indices of the modified design curve P_{TEST}/P_{DSM}^M from Eq. (7) is 3.25 and 3.30 which are higher than the target reliability index value suggested by AISI (2020), indicating that the modified curve (Eq. 7) is suitable for the axial strength prediction of CFS doubly symmetric built-up column with interactive local-global buckling modes. A higher value of the reliability index was necessary to achieve a conservative design as the magnitude of the coefficient of variation is high.

Although this investigation is a preliminary validation study for the use of AISI DSM curves for the design of CFS doubly-symmetric built-up cross-sections, more investigation is required to further improve the user-friendliness of the DSM for various shapes and failure modes of the CFS built-up members. Future investigation may focus on the analysis of structural behavior of the complex and/or simple but unstable CFS cross-sections which the industry needs (i.e. built-up assembly with more than two individual cross-sections). When more experimental data become available for the built-up cross-section assembly columns, the DSM may accommodate such results by (i) introducing a resistance factor (ϕ) for each cross-section; (ii) including more definite prequalification limits; (iii) formulate a modified slenderness expression [28] to make the DSM user-friendly. In addition, it is suggested that the DSM design procedure shall have an appropriate commentary section elucidating the various possible failure modes of the CFS built-up doubly-symmetric columns, as it will engage the average design engineer to calculate the flexural torsional buckling stress who otherwise might not consider the possible occurrence of the flexural torsional buckling for a doubly symmetric built-up section with intermediate spacing (a) and may have performed a finite strip analysis (recommended by Young and Chan [13]) which is an easy option. The authors of this paper committed to develop accurate and robust design methods for the cold-formed steel members, for example Direct Stiffness-Strength Method [29-46].

Parameter		Eq. (6)	Eq. (8)
$\dfrac{P_{EXP}}{P_{DSM}}$	Mean	0.9	1.1
	Max	1.04	1.28
	Min	0.74	0.91
	β_1	2.38	3.25
	β_2	2.42	3.30

Fig.5. (a) Comparison of test results with AISI (2020) and modified design curve; (b) Appropriateness of Modified interactive local buckling curve

7 Conclusions

The axial compression test results of the cold-formed steel back-to-back connected doubly symmetric built-up cross-section assemblies are presented. The test parameters include slenderness of the CFS section (λ_l and λ_e), length of the column (L), and intermediate spacing (*a*). The ultimate axial strength and corresponding failure modes of the tested columns are presented with an appropriate interpretation for understanding. Based on the test and design results, the following conclusions can be drawn:

1. The test results indicate that the back-to-back connected doubly symmetric built-up cross-section assembly columns failed predominantly in interactive local and flexural-torsional buckling. The influence of intermediate fastener spacing was prevalent in the failure modes of the doubly symmetric CFS built-up columns.
2. It is demonstrated experimentally that the shift in the line of action of the internal force caused by local buckling deformations does induce global instability (overall flexural torsional buckling) in fixed-ended columns. This is the main reason for local-global interaction buckling and results in significant column strength reduction compared to the individual local buckling strength.
3. AISI's maximum intermediate connection spacing limitation $[(a/r_i) \leq 0.5 (KL/r)_o]$ is appropriate (overly safe) to prevent global instability failures (individual section buckling) in the built-up assemblies with predominant interactive local-global failure mode vulnerability.
4. The comparison between the test results and design predictions indicated that the current AISI's design curve for interactive buckling is unconservative for the CFS built-up columns with predominant interactive local-global failure mode vulnerability.
5. A modified design curve for interactive buckling is formulated based on the test results and found to be conservative for design application. The reliability analysis of the new design curve is also demonstrated.

The improvements in the DSM method with respect to the CFS built-up structural members and intermediate fastener spacing can be expected in near future from the present authors.

References

1. Camotim, D., Martins, A.D., Dinis, P.B., Young, B., Chen, M.T. and Landesmann, A., (2021). Mode Interaction in Cold-Formed Steel Members: State-of-Art Report. ce/papers, 4(2-4), pp.34-64.
2. AISI. (American Iron and Steel Institute) (2020). "North American Cold-Formed Steel Specification for the Design of Cold-Formed Steel Structural Members." AISI-S100-2016 edition (Reaffirmed 2020) with supplement 2, Washington, DC.
3. Schafer, B.W., (2008). The direct strength method of cold-formed steel member design. Journal of constructional steel research, 64(7-8), pp.766-778.
4. Yang D, Hancock GJ (2004). Compression tests of high strength steel channel columns with interaction between local and distortional buckling, Journal of Structural Engineering (ASCE), 130(12), 1954-1963.
5. Young B, Silvestre N, Camotim D (2013). Cold-formed steel lipped channel columns influenced by local-distortional interaction: strength and DSM design, Journal of Structural Engineering (ASCE), 139(6), 1059-1074.
6. Dinis PB, Young B, Camotim D (2014). Local-distortional interaction in cold-formed steel rack-section columns, Thin-Walled Structures, 81, 185-194.
7. Anbarasu M (2016). Local-distortional buckling interaction on cold-formed steel lipped channel beams, Thin-Walled Structures, 98B, 351-359.
8. Martins AD, Camotim D, Dinis PB (2017). On the direct strength design of cold-formed steel columns failing in local-distortional interactive modes, Thin-Walled Structures, 120, 432-445.
9. Selvaraj, S. and Madhavan, M., 2019. Structural design of cold-formed steel face-to-face connected built-up beams using direct strength method. Journal of Constructional Steel Research, 160, pp.613-628.
10. Selvaraj, S. and Madhavan, M., 2020. Cold-formed steel built of columns: Experimental investigation. Hong Kong Institution of Steel Construction, https://doi.org/10.18057/ICASS2018.P.168.
11. Selvaraj, Sivaganesh, and Mahendrakumar Madhavan. "Design of cold-formed steel back-to-back connected built-up beams." Journal of Constructional Steel Research 181 (2021): 106623.
12. Selvaraj, S. and Madhavan, M., 2021. Direct strength approach for local buckling of cold-formed steel built-up beams with slender unstiffened flange elements. Practice Periodical on Structural Design and Construction, 26(3), p.06021004.
13. Young, B., and Chen, J. (2008). Design of cold-formed steel built-up closed sections with intermediate stiffeners. Journal of Structural Engineering, 134(5), 727-737.
14. Camotim, D., Martins, A.D., Dinis, P.B., Young, B., Chen, M.T. and Landesmann, A., (2020). Mode interaction in cold-formed steel members: state-of-art report: Part 1: Fundamentals and local-distortional coupling. Steel Construction, 13(3), pp.165-185.

15. Camotim, D., Martins, A.D., Dinis, P.B., Young, B., Chen, M.T. and Landesmann, A., (2020). Mode interaction in cold-formed steel members: state-of-art report: Part 2: Couplings involving global buckling. Steel Construction, 13(3), pp.186-207.

16. Selvaraj, S. and Madhavan, M., 2022. Experimental investigation and design considerations on cold-formed steel built-up I-section columns subjected to interactive buckling modes. Thin-Walled Structures, 175, p.109262.

17. Selvaraj, S. and Madhavan, M., 2021. Design of cold-formed steel built-up columns subjected to local-global interactive buckling using direct strength method. Thin-Walled Structures, 159, p.107305.

18. Martins AD, Landesmann A, Camotim D, Dinis PB (2017). Distortional failure of cold-formed steel beams under uniform bending: behaviour, strength and DSM design, Thin-Walled Structures, 118, 196-213.

19. Dinis PB, Camotim D, Landesmann A, Martins AD (2020). Improving the Direct Strength Method prediction of column flexural-torsional failure loads, Thin-Walled Structures, 148, paper 106461.

20. Selvaraj, S. and Madhavan, M., 2018. Geometric imperfection measurements and validations on cold-formed steel channels using 3D noncontact laser scanner. Journal of Structural Engineering, 144(3), p.04018010.

21. Loughlan, J. and Nabavian, M., "The Behaviour of Thin-walled I-section Columns After Local Buckling" (1986). International Specialty Conference on Cold-Formed Steel Structures. 2.

22. Mulligan, Gale P. and Peköz, Teoman, "The influence of local buckling on the structural behavior of singly symmetric cold-formed steel columns" (1983). Center for Cold-Formed Steel Structures Library. 117.

23. Young, B. and Rasmussen, K.J., 1999a. Behaviour of cold-formed singly symmetric columns. Thin-walled structures, 33(2), pp.83-102.

24. Young, B., and Rasmussen, K. J. (1999). Shift of effective centroid of channel columns. Journal of Structural Engineering, 125(5), 524-531.

25. Rasmussen, K.J.R. and Hancock, G.J., (1993). The flexural behaviour of fixed-ended channel section columns. Thin-walled structures, 17(1), pp.45-63.

26. ASCE, Minimum design loads for buildings and other structures, ASCE/SEI 7–10, ASCE, Reston, VA, 2010.

27. AS/NZS 4600:2005. Cold-formed steel structures. Standards Australia.

28. Selvaraj, S. and Madhavan, M., (2022). Design of Cold-formed Steel Built-Up Closed Section Columns using Direct Strength Method. Thin-Walled Structures, 171, p.108746.

29. Selvaraj, S. and Madhavan, M., 2019. Improvements in AISI design methods for gypsum-sheathed cold-formed steel wall panels subjected to bending. Journal of Structural Engineering, 145(2), p.04018243. https://doi.org/10.1061/(ASCE)ST.1943-541X.0002223

30. Selvaraj, S. and Madhavan, M., 2017. 07.24: Behaviour of gypsum sheathed cold-formed steel stud walls under lateral loadings. ce/papers, 1(2-3), pp.1707-1715. https://doi.org/10.1002/cepa.214

31. Selvaraj, S. and Madhavan, M., 2019. Behaviour and Design of Sheathed Cold-formed Steel Wall Studs subjected to Torsional Buckling. PhD thesis, Indian Institute of Technology Hyderabad. http://raiith.iith.ac.in/id/eprint/5744.

32. Selvaraj, S. and Madhavan, M., 2019. Investigation on sheathing effect and failure modes of gypsum sheathed cold-formed steel wall panels subjected to bending. Structures (Vol. 17, pp. 87-101). Elsevier. https://doi.org/10.1016/j.istruc.2018.09.013

33. Selvaraj, S. and Madhavan, M., 2019. Sheathing braced design of cold-formed steel structural members subjected to torsional buckling. Structures (Vol. 20, pp. 489-509). Elsevier. https://doi.org/10.1016/j.istruc.2019.04.015

34. Selvaraj, S. and Madhavan, M., 2019. Investigation on sheathing-fastener connection failures in cold-formed steel wall panels. Structures (Vol. 20, pp. 176-188). Elsevier. https://doi.org/10.1016/j.istruc.2019.03.007

35. Selvaraj, S. and Madhavan, M., 2019. Flexural behaviour and design of cold-formed steel wall panels sheathed with particle cement board. Journal of Constructional Steel Research, 162, p.105723. https://doi.org/10.1016/j.jcsr.2019.105723

36. Selvaraj, S. and Madhavan, M., 2020. Structural behaviour and design of plywood sheathed cold-formed steel wall systems subjected to out of plane loading. Journal of Constructional Steel Research, 166, p.105888. https://doi.org/10.1016/j.jcsr.2019.105888

37. Selvaraj, S. and Madhavan, M., 2020. Recommendations for design of sheathing bracing systems for slender cold-formed steel structural members. Journal of Constructional Steel Research, 170, p.106116. https://doi.org/10.1016/j.jcsr.2020.106116

38. Selvaraj, S. and Madhavan, M., 2020. Influence of sheathing-fastener connection stiffness on the design strength of cold-formed steel wall panels. Journal of

Structural Engineering, 146(10), p.04020202. https://doi.org/10.1061/(ASCE)ST.1943-541X.0002709

39. Selvaraj, S., Madhavan, M. and Lau, H.H., 2021. Sheathing-fastener connection strength based design method for sheathed CFS point-symmetric wall frame studs. Structures (Vol. 33, pp. 1473-1494). Elsevier. https://doi.org/10.1016/j.istruc.2021.04.052

40. Madhavan, M., and Selvaraj, S. 2022. Direct stiffness–strength method design for cold-formed steel structural members with sheathing bracing. Analysis and Design of Plated Structures, Woodhead Publishing, 437-478. https://doi.org/10.1016/B978-0-12-823570-6.00005-7

41. Selvaraj, S. and Madhavan, M., 2021. Stiffness based design method for sheathed cold-formed steel members subjected to torsional buckling. Proceedings of the Annual Stability Conference Structural Stability Research Council 2021, SSRC 2021, Structural Stability Research Council.

42. Selvaraj, S. and Madhavan, M., 2018. Studies on cold-formed steel stud panels with gypsum sheathing subjected to out-of-plane bending. Journal of Structural Engineering, 144(9), p.04018136. https://doi.org/10.1061/(ASCE)ST.1943-541X.0002069

43. Selvaraj, S. and Madhavan, M., 2019. Sheathing bracing requirements for cold-formed steel wall panels: Experimental investigation. Structures (Vol. 19, pp. 258-276). https://doi.org/10.1016/j.istruc.2019.01.005

44. Selvaraj, S. and Madhavan, M., 2019. Bracing effect of sheathing in point-symmetric cold-formed steel flexural members. Journal of Constructional Steel Research, 157, pp.450-462. https://doi.org/10.1016/j.jcsr.2019.02.037

45. Selvaraj, S. and Madhavan, M., 2019. Behaviour of Gypsum Sheathed Point-symmetric Cold-formed Steel members: Assessment of AISI Design Method. Structures (Vol. 22, pp. 76-97). https://doi.org/10.1016/j.istruc.2019.06.005

46. Selvaraj, S. and Madhavan, M., 2021. Direct stiffness-strength method design for sheathed cold-formed steel structural members-Recommendations for the AISI S100. Thin-Walled Structures, p.107282. https://doi.org/10.1016/j.tws.2020.107282